Valley-Polarized Quantum Hall Phase in a Strain-Controlled Dirac System

G. Krizman,[1,*] J. Bermejo-Ortiz,[2] T. Zakusylo,[1] M. Hajlaoui,[1] T. Takashiro,[1] M. Rosmus,[3] N. Olszowska,[3] J. J. Kołodziej,[3,4] G. Bauer,[1] Y. Guldner,[2] G. Springholz,[1] and L.-A. de Vaulchier[2]

[1]*Institut für Halbleiter und Festkörperphysik, Johannes Kepler Universität, Altenberger Strasse 69, 4040 Linz, Austria*

[2]*Laboratoire de Physique de l'Ecole normale supérieure, ENS, Université PSL, CNRS, Sorbonne Université, 24 rue Lhomond 75005 Paris, France*

[3]*National Synchrotron Radiation Centre SOLARIS, Jagiellonian University, Czerwone Maki 98, 30-392 Krakow, Poland*

[4]*Faculty of Physics, Astronomy and Applied Computer Science, Jagiellonian University, 30-348 Krakow, Poland*

(Received 15 December 2023; revised 21 February 2024; accepted 27 March 2024; published 16 April 2024)

In multivalley systems, the valley pseudospin offers rich physics going from encoding of information by its polarization (valleytronics), to exploring novel phases of matter when its degeneracy is changed. Here, by strain engineering, we reveal fully valley-polarized quantum Hall phases in the $Pb_{1-x}Sn_xSe$ Dirac system. Remarkably, when the valley energy splitting exceeds the fundamental band gap, we observe a "bipolar quantum Hall phase," heralded by the coexistence of hole and electron chiral edge states at distinct valleys in the same quantum well. This suggests that spatially overlaid counterpropagating chiral edge states emerging at different valleys do not interfere with each other.

DOI: 10.1103/PhysRevLett.132.166601

Quantum Hall (QH) phases have been inspiring and generating a large amount of original physics for more than 40 years [1,2]. In particular, multivalley systems have attracted major interest for the discovery of novel phases of matter [3–6]. The valley degree of freedom accounts for a pseudospin that considerably enriches the QH phase, like the SU(2) or SU(4) QH ferromagnetisms observed in graphene [7–10] or AlAs [11–13]; or the QH nematic phases recently discovered in the AlAs/AlGaAs system [14] and at the Bi (111) surface [15]. In the $Pb_{1-x}Sn_xSe/Te$ QH system, the valley degeneracy is predicted to yield a rare SU(3) QH ferromagnetism analogous to the quark model, and a nematic phase [4,5]. Such exotic phases are the setting for intriguing physical phenomena involving many-body interactions [4,5,7] and can host topological excitations like anyons [16–18], skyrmions [5,19], or charge density waves [20,21].

The valley degree of freedom has also created a new paradigm for (quantum) information processing [22–25]. Valleytronics thereby refers to the use and manipulation of the valley pseudospin to carry and store the information, which is actively studied for AlAs [12,26,27], diamond [28], the Si and Si/Ge systems [25,29–31], graphene [24,32,33], and 2D materials like WSe_2 or MoS_2 [23,34,35]. These materials have shown valley-selective interactions with applied optical, electric, or mechanical fields that renders them potential candidates for device applications [34]. The key for efficient valleytronic effects relies on finding robust and switchable valley-polarized states in wafer-scale materials that can be controlled by external knobs in order to drive carriers selectively at different momenta [36].

By revealing an extremely large valley energy splitting induced by strain, we show that the multivalley $Pb_{1-x}Sn_xSe$ system presents indisputable qualities for monitoring the valley degree of freedom and is a serious candidate for both the discovery of spontaneous valley-symmetry breaking as well as valleytronic applications. $Pb_{1-x}Sn_xSe$ (111)-oriented quantum wells (QWs) host four Fermi pockets [see Fig. 1(a)]: one isotropic longitudinal valley (l) located at the $\bar{\Gamma}$ point, and three equivalent oblique valleys (o) at the $\bar{M}$ points [4,37,38] that are anisotropic and related by a $\mathcal{C}_3$ rotational symmetry. This system exhibits a fundamental band gap with electron-hole symmetry in all valleys [39,40]. Controlling the population of the different valleys is crucial for accessing novel phases of matter through spontaneous valley-symmetry breaking and for the development of valley-polarized transport for valleytronics technologies.

In this Letter, by measuring the integer QH effect on QWs grown along the [111] direction [Fig. 1(b)], we reveal a strong dependence of the valley splitting Δ_{l-o} on the in-plane biaxial strain. By controlling strain and doping levels, the PbSnSe QH system shows the emergence of several distinct transport regimes summarized by the QH phase diagram plotted in Fig. 1(c). When the strain, and thus the valley splitting Δ_{l-o} are small, quantum transport occurs in both types of valleys with the same type of carriers [41–43].

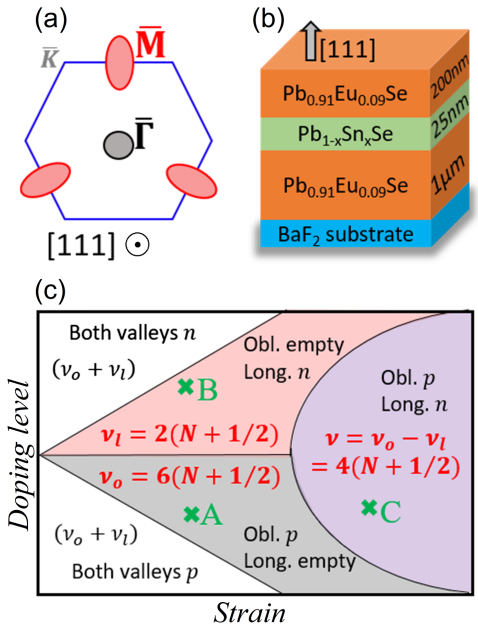

FIG. 1. (a) Brillouin zone of $Pb_{1-x}Sn_xSe$ projected onto the (111) surface. The $\bar{\Gamma}$ and $\bar{M}$ valleys are shown in black and red. (b) Structure of the investigated QW samples. (c) Valleytronic phase diagram as a function of Fermi level and in-plane biaxial strain. Valley-polarized (red and black) and bipolar (purple) QH phases manifest themselves by different plateau filling factors. N denotes the Landau level index. The investigated samples A, B, and C are placed according to their properties.

For small but nonzero strain values, the valley splitting is such that, depending on the Fermi level, a fully valley-polarized state emerges. In this regime, we demonstrate that strain can monitor the valley-pseudospin of Dirac fermions. Last but not least, a bipolar regime is observed when Δ_{l-o} becomes larger than the band gap 2δ of the QW, yielding hole and electron edge channels to coexist in the same QW layer but within different valleys.

Control of strain and doping levels.—The key parameter in our Letter is the in-plane biaxial strain, which we control by adjusting the lattice mismatch between the buffer and QW layers. Samples are grown by molecular beam epitaxy on BaF_2 substrates and consist of 25 nm thick (111)-oriented $Pb_{1-x}Sn_xSe$ QWs with different compositions and doping levels embedded between undoped and relaxed $Pb_{0.91}Eu_{0.09}Se$ buffer and capping layers [see Fig. 1(b) and Supplemental Material [44]]. The pseudomorphic growth is demonstrated by x-ray diffraction shown in [44]. As a result, the QWs are under biaxial tensile strain, whose magnitude is governed by the Sn concentration [44] (see Table I). The second varied parameter is the doping level. It is controlled *in situ* during the growth by Bi doping, which acts as a donor and compensates the native hole concentration naturally present in $Pb_{1-x}Sn_xSe$ [45]. The existence of the different QH phases [see Fig. 1(c)] is demonstrated by means of three samples A, B, and C exhibiting different strains, band gaps and doping levels listed in Table I. All samples were patterned in 1×0.3 mm^2 Hall bars [43]. The contacts were made by indium soldering and the Hall measurements were carried out at $T = 1.6$ K up to $B = 17$ T.

Valley-polarized QH regimes.—Figure 2 shows the QH effect measured in samples A and B which host $Pb_{1-x}Sn_xSe$ QWs with $x \sim 9\%$. Both QWs are under tensile strain with $\varepsilon_{\parallel} \sim 0.44\%$ and their carrier densities lie below 10^{12} cm^{-2} (see Table I). Both samples present precisely quantized Hall plateaus with vanishing longitudinal resistances, depicting a clear QH phase. For the p-type sample A [Fig. 2(a)], the observed QH plateaus exhibit plateaus at $-h/\nu e^2$ with filling factors $\nu = 3$ and 9, as well as a small feature at $\nu = 15$ (see the derivative in [44]). For n-type sample B [Fig. 2(b)] the most pronounced plateaus are seen for $\nu = 1$ and 3, with small additional features at $\nu = 2$ and 4.

Figure 2 demonstrates the fully valley-polarized transport regimes that $Pb_{1-x}Sn_xSe$ can provide. The different degeneracy of the Landau levels below the Fermi energy is responsible for the observed filling factors. In sample A, a transition from filling factor 9 to 3 means that the Landau levels are sixfold degenerate. Considering the two spins, this yields a threefold valley degeneracy, meaning that only the three oblique valleys are populated and contribute to the quantum transport. In sample B, despite having the same strain status and Sn content (see Table I), the situation is completely different due to the different carrier type stemming from the distinct Bi doping during the growth. For this reason, only the single longitudinal valley is

TABLE I. Characteristics at $T = 1.6$ K of the investigated samples. All QWs are 25 nm thick.

Samples	A	B	C	
x_{Sn} (%)	8.5 ± 1	9 ± 1	15 ± 1	
$\varepsilon_{\parallel}$ (%)	0.46 ± 0.04	0.42 ± 0.04	0.62 ± 0.04	
2δ (meV)	92 ± 2.5	83 ± 2.5	50 ± 2.5	
Δ_{l-o} (meV)	74[a]	67[a]	92 ± 5	
Doping (cm^{-2})	$p^\circ = 7.45 \times 10^{11}$	$n^l = 3.54 \times 10^{11}$	$n^l = 1.81 \times 10^{11}$	$p^\circ = 5.42 \times 10^{11}$
Filling factor series	$\nu_o = 6(N + 1/2)$	$\nu_l = 2(N + 1/2)$	$\nu_o - \nu_l = 4(N + 1/2)$	
Mobility (cm^2/V.s)	$\mu_h = 37\,800 \pm 2000$	$\mu_e = 37\,000 \pm 2000$	$\mu_e = 150\,000 \pm 20\,000$	$\mu_h = 55\,000 \pm 5000$

[a]Deduced from Eq. (1).

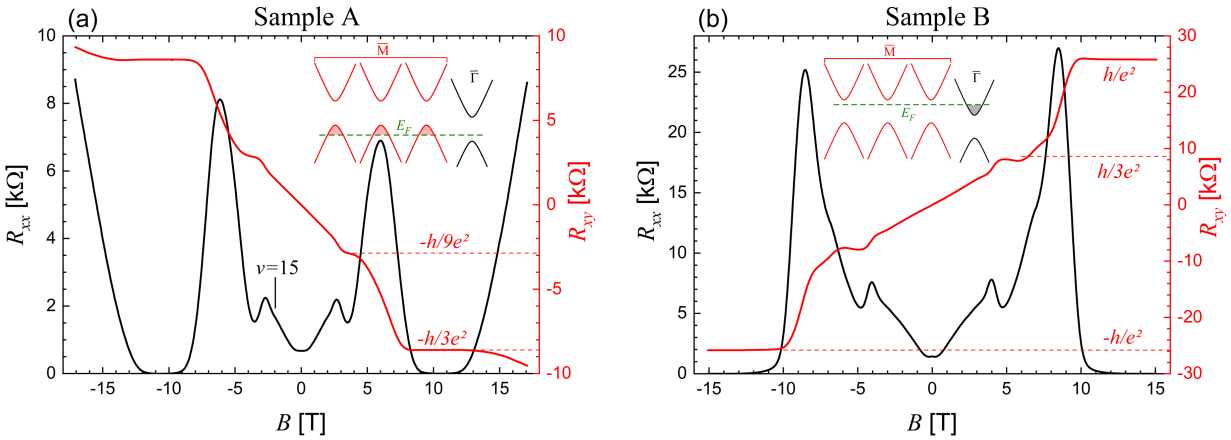

FIG. 2. QH effect measured in sample A (holes) (a) and B (electrons) (b) at $T = 1.6$ K. The dashed red lines indicate the calculated plateau values. The insets illustrate the strained multivalley band structures with the corresponding Fermi level.

populated, which is witnessed by the features observed for $\nu = 3$ and $\nu = 1$. The valley alignment and Fermi levels of the two samples are schematically depicted in the insets of Fig. 2 and illustrate the fully valley-polarized QH regime.

Interestingly, the QH plateaus observed in samples A and B display Dirac-like Landau levels: the Zeeman splitting is equal to the cyclotron energy and thus, the $N = 0\uparrow$ Landau level is degenerate with $N = 1\downarrow$, leaving a spin-polarized $N = 0\downarrow$ ground Landau level. This gives the well-known Dirac filling factor series $\nu = g_s g_v(N + 1/2)$, with g_s and g_v being the spin and valley degeneracies, respectively [46,47]. Here, $g_v = 1$ ($g_v = 3$) corresponds to the valley-polarized regime where only the $\bar{\Gamma}$ valley (threefold degenerated $\bar{M}$ valleys) is populated. In both cases, this promotes plateaus with *odd* filling factors as we experimentally observe. For sample A, the observed plateaus appear at $\nu_o = 6(N + 1/2)$, that is reminiscent of graphene's, however, with a different valley degeneracy. Sample B shows a single-valley Dirac behavior with $\nu_l = 2(N + 1/2)$. This clearly characterizes the PbSnSe system as a Dirac material with a strain tunable multivalley character.

The bipolar QH effect.—The third investigated QH phase occurs when the valley splitting exceeds the QW gap, i.e., $\Delta_{l-o}(\varepsilon_\parallel) > 2\delta$. This requires a relatively high strain and/or a small gap value. Here, we have quantified the valley splitting as a function of strain $\Delta_{l-o}(\varepsilon_\parallel)$ using angle-resolved photoemission spectroscopy (ARPES). For this purpose, additional samples were grown with a much higher doping level and without capping layer, leaving a 20 nm $Pb_{1-x}Sn_xSe$ QW layer exposed at the surface. Different strains were realized by changing the Sn content from 0% to 25%, which changes the lattice mismatch with respect to their underlying PbSe buffer and yields $\varepsilon_\parallel$ from 0% to 0.5%, respectively. Band maps in the vicinity of the $\bar{\Gamma}$ and $\bar{M}$ points were measured for each sample [Figs. 3(a)

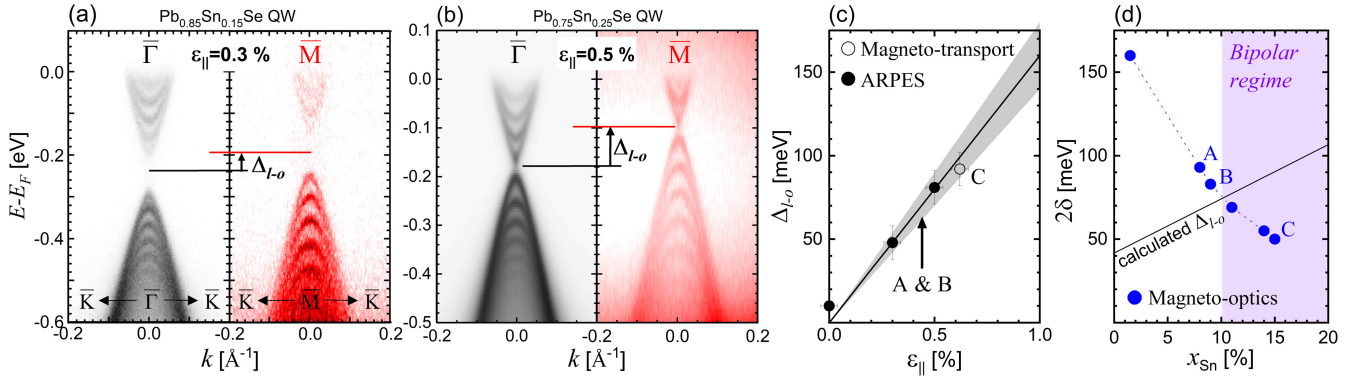

FIG. 3. (a),(b) ARPES band maps of the confined subbands in strained 20 nm $Pb_{1-x}Sn_xSe$ QWs at the $\bar{\Gamma}$ and $\bar{M}$ points for different strain values. The valley splitting Δ_{l-o} is indicated by the horizontal black and red lines. (c) Valley splitting as a function of in-plane biaxial strain deduced from ARPES and transport. The linear fit with Eq. (1) and error bars on D_u are represented by the solid line and the shaded area. (d) QW gaps versus Sn content determined by magneto-optics. Blue dashed line is a guide for the eye. The black line corresponds to the calculated valley splitting. The crossing between blue and black lines delimits the bipolar regime (purple shaded area).

and 3(b) and [44]]. In each case, a large number of sharp quantum confined states is observed both in the conduction and valence bands.

The ARPES measurements allow us to accurately determine $\Delta_{l-o}(\varepsilon_{\parallel})$. This is achieved by measuring the energy difference between the neutral points (middle of the gap) at $\bar{\Gamma}$ and $\bar{M}$ as indicated in Figs. 3(a) and 3(b). The results are summarized in Fig. 3(c). The dependence of $\Delta_{l-o}(\varepsilon_{\parallel})$ can be computed [48,49] using the relation

$$\Delta_{l-o} = \frac{8}{9}(1+\lambda)D_u\varepsilon_{\parallel}, \tag{1}$$

where λ is the Poisson ratio and D_u the uniaxial deformation potential. Taking the value of $\lambda = 1.162$ of PbSe [50], we deduce $D_u = 8.3 \pm 1$ eV [see Fig. 3(c)], in fair agreement with literature [51–53]. Overall, this yields $\Delta_{l-o} = 16\varepsilon_{\parallel}$ in eV, evidencing a valley splitting that is highly strain sensitive. Note that the gap is found to be essentially equal at the $\bar{\Gamma}$ and $\bar{M}$ points.

The QW band gaps $2\delta(x)$ of samples A, B, and C have been measured by magnetoinfrared spectroscopy following the procedure detailed in Refs. [38,39,44]. This determination includes the strain, composition, and quantum confinement contributions to the gap. The results are plotted in Fig. 3(d) and show the decrease of the gap with increasing Sn content due to the emergent topological crystalline phase in $Pb_{1-x}Sn_xSe$ for $x > 16\%$ [54,55]. The outstanding tuning range of the valley splitting and gap of $Pb_{1-x}Sn_xSe$ allows us to realize the condition $\Delta_{l-o}(\varepsilon_{\parallel}) > 2\delta(x)$ and to reach the bipolar QH regime [see Fig. 3(d)]. Indeed, sample C fulfills this criterium as its magneto-optics gives $2\delta = 50$ meV, with a relatively large strain value ($\varepsilon_{\parallel} = +0.62\%$) corresponding to $\Delta_{l-o} = 99$ meV using Eq. (1). Its transport curves are shown in Fig. 4(a) and its calculated Landau levels in Fig. 4(b) using the parameters determined in magneto-optics. The band structure is also depicted in the inset of Fig. 4(a), where one electron pocket lies at $\bar{\Gamma}$, and three hole pockets at $\bar{M}$. Using a two-carrier model [44,56], the hole concentration is found three times higher than that of the electrons, meaning that each valley hosts about the same number of carriers (see Table I). Therefore, the Landau levels associated with electrons (at $\bar{\Gamma}$) and those with holes (at $\bar{M}$) cross the Fermi level simultaneously. This special configuration allows us to observe clear QH plateaus at filling factors 10, 6, and 2 as R_{xx} goes to 0 for both valleys at the same time. These observed plateaus can be explained if one considers that different types of carriers are present in the two types of valleys, resulting in

$$\nu = \nu_o - \nu_l = g_s(g_{v,o} - g_{v,l})(N + 1/2) = 4(N + 1/2).$$

The contributions of all valleys add up to lead to the observed QH plateaus with $\nu = \nu_o - \nu_l = 3 - 1 = 2$; $\nu = 9 - 3 = 6$ and then for $\nu = 15 - 5 = 10$. The Landau level calculations together with the measured carrier concentrations allow us to conclude that $\Delta_{l-o} = 92$ meV for this sample, in perfect agreement with our ARPES study [see Fig. 3(c) and Eq. (1)].

At high magnetic field, this configuration yields a $\nu = 2$ plateau that would be formed by three hole chiral edge states (one per oblique valley) coexisting with the single electron chiral edge state of the longitudinal valley, as illustrated in Figs. 4(c) and 4(d). Remarkably, our observation shows that a dissipationless QH effect still persists. This would evidence that the counterpropagating hole and electron chiral states from different valleys do not interfere with each other but rather add up in their contribution. This observation is puzzling and asks for further study.

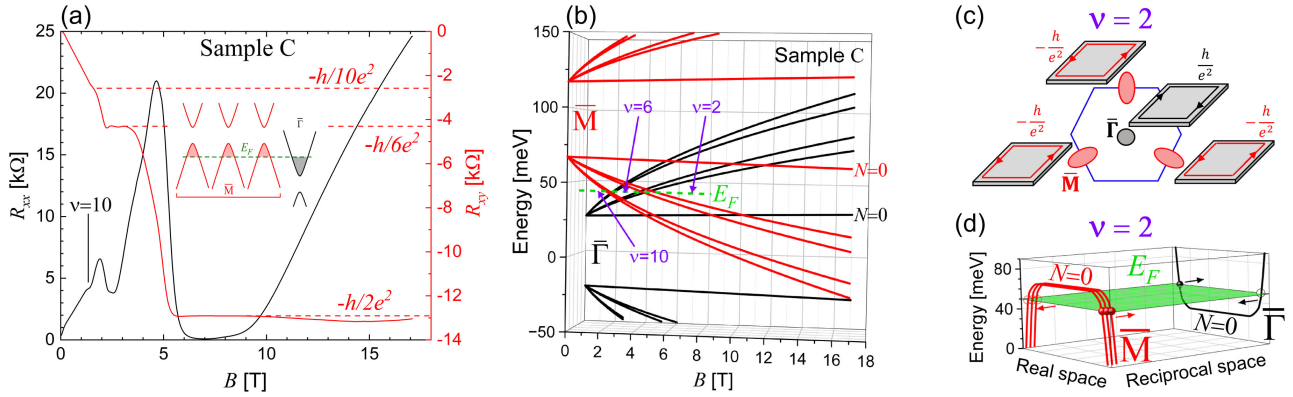

FIG. 4. (a) QH measurements of sample C at $T = 1.6$ K. The inset illustrates the multivalley band alignment and the Fermi level. (b) Corresponding calculated Landau levels emerging at $\bar{M}$ (red at the front) and $\bar{\Gamma}$ (black at the back). The Fermi level as well as the observed filling factor series are indicated. (c) Schematic illustration of the 2D Brillouin zone with the counterpropagating edge channels in different valleys giving $\nu = -2$. (d) Scheme of the $N = 0$ Landau levels in real space at $\bar{M}$ (red at the front) and $\bar{\Gamma}$ (black at the back) and the Fermi level leading to $\nu = -2$. The right-handed (left-handed) chiral edge states are indicated by filled (empty) circles.

We want to emphasize that the counterpropagating chiral edge states probed here are well separated in the reciprocal space but coincide in real space as represented in Figs. 4(c) and 4(d). This is unique and differs from any previous works, in particular from the QH effect observed in InAs/GaSb heterostructures where electron and hole chiral states are both localized at the center of the Brillouin zone and occur in spatially separated layers [57]. This situation creates hybridizations between electron and hole 2D states [58], as well as interactions between electron and hole 1D edge states [59]. A related situation occurs also in graphene where, at $\nu = 0$, a dissipative QH effect is measured [10,60]. However, the gaps between the four $N = 0$ Landau levels are rather small (∼meV) [10] compared to the ∼45 meV found here in sample C. Moreover, the $\nu = 0$ plateau of graphene cannot possibly exhibit the usual QH hallmarks as it would theoretically lead to $\rho_{xx} = \rho_{xy} = 0$, which would denote a superconducting state [60–62].

In summary, our Letter has revealed the rich QH phases accessible in $Pb_{1-x}Sn_xSe$. By demonstrating Dirac-like plateaus at $\nu_o = 6(N + 1/2)$ and $\nu_l = 2(N + 1/2)$, we show fully polarized valley pseudospin of Dirac fermions. This is made possible by a strain-control of the valley splitting ($\Delta_{l-o} = 16\varepsilon_{\parallel}$ eV) and is promising for PbSnSe-based valleytronics devices like valley filter or valve [24,37], and quantum information storage [22,23,25,28]. To go further, one can grow or transfer the PbSnSe QW layers on a piezoelectric substrate. In this way, the strain induced valley-splitting would be simply driven by an external electric field.

The valley-polarized regime is also of primary interest for the exploration of new exotic phases of matter like nematics, QH ferroelectricity, and SU(3) QH ferromagnetism [4,5]. Indeed, the possibility to drive the QH effect independently in one type of valley or the others allows for varying the Landau levels degeneracy. In this way, sample A stands as an ideal platform to access an SU(3) QH ferromagnetism, since only the threefold degenerate oblique valleys are populated [4]. As proposed in Ref. [4], one can also use an additional in-plane magnetic field to lift the valley degeneracy and access the SU(3) QH ferromagnetic phase.

Finally, the QH effect has been measured when both types of valleys are populated with different types of carriers, introducing an intriguing bipolar QH phase. In this regime, electron and hole chiral states emerging within different valleys coexist in a single QW and give plateaus at filling factors that are the sum of involved electron and hole chiral edge states. This would mean that no interactions occur between counterpropagating chiral states located at different momenta of the Brillouin zone but coinciding in real space, an observation that should certainly deserve theoretical attention.

The authors thank T. Ihn for enlightening discussions, as well as J. Palomo and U. Kainz for technical assistance. We acknowledge support by the French Agence Nationale de la Recherche (ANR, Contract No. ANR-19-CE30-022-01) and the Austrian Science Funds (FWF, Project No. I-4493). The ARPES setup was developed under the provision of the Polish Ministry and Higher Education project Support for research and development with the use of research infra-structure of the National Synchrotron Radiation Centre "SOLARIS" under Contract No. 1/SOL/2021/2.

*Corresponding author: gauthier.krizman@jku.at

[1] K. V Klitzing, G. Dorda, and M. Pepper, New method for high-accuracy determination of the fine-structure constant based on quantized Hall resistance, Phys. Rev. Lett. **45**, 494 (1980).
[2] K. von Klitzing *et al.*, 40 years of the quantum Hall effect, Nat. Rev. Phys. **2**, 397 (2020).
[3] M. T. Randeria, B. E. Feldman, F. Wu, H. Ding, A. Gyenis, H. Ji, R. J. Cava, A. H. MacDonald, and A. Yazdani, Ferroelectric quantum Hall phase revealed by visualizing Landau level wavefunction interference, Nat. Phys. **14**, 796 (2018).
[4] X. Li, F. Zhang, and A. H. MacDonald, SU(3) quantum Hall ferromagnetism in SnTe, Phys. Rev. Lett. **116**, 026803 (2016).
[5] I. Sodemann, Z. Zhu, and L. Fu, Quantum Hall ferroelectrics and nematics in multivalley systems, Phys. Rev. X **7**, 041068 (2017).
[6] D. A. Abanin, S. A. Parameswaran, S. A. Kivelson, and S. L. Sondhi, Nematic valley ordering in quantum Hall systems, Phys. Rev. B **82**, 035428 (2010).
[7] K. Nomura and A. H. MacDonald, Quantum Hall ferromagnetism in graphene, Phys. Rev. Lett. **96**, 256602 (2006).
[8] A. F. Young, C. R. Dean, L. Wang, H. Ren, P. Cadden-Zimansky, K. Watanabe, T. Taniguchi, J. Hone, K. L. Shepard, and P. Kim, Spin and valley quantum Hall ferromagnetism in graphene, Nat. Phys. **8**, 550 (2012).
[9] X. Liu, G. Farahi, C.-L. Chiu, Z. Papic, K. Watanabe, T. Taniguchi, M. P. Zaletel, and A. Yazdani, Visualizing broken symmetry and topological defects in a quantum Hall ferromagnet, Science **375**, 321 (2022).
[10] Y. Zhang, Z. Jiang, J. P. Small, M. S. Purewal, Y.-W. Tan, M. Fazlollahi, J. D. Chudow, J. A. Jaszczak, H. L. Stormer, and P. Kim, Landau-level splitting in graphene in high magnetic fields, Phys. Rev. Lett. **96**, 136806 (2006).
[11] E. P. De Poortere, E. Tutuc, S. J. Papadakis, and M. Shayegan, Resistance spikes at transitions between quantum Hall ferromagnets, Science **290**, 1546 (2000).
[12] M. Shayegan, E. P. De Poortere, O. Gunawan, Y. P. Shkolnikov, E. Tutuc, and K. Vakili, Two-dimensional electrons occupying multiple valleys in AlAs, Phys. Status Solidi (b) **243**, 3629 (2006).
[13] Md. S. Hossain, M. K. Ma, Y. J. Chung, S. K. Singh, A. Gupta, K. W. West, K. W. Baldwin, L. N. Pfeiffer, R. Winkler, and M. Shayegan, Fractional quantum Hall valley ferromagnetism in the extreme quantum limit, Phys. Rev. B **106**, L201303 (2022).
[14] N. Samkharadze, K. A. Schreiber, G. C. Gardner, M. J. Manfra, E. Fradkin, and G. A. Csáthy, Observation of a

transition from a topologically ordered to a spontaneously broken symmetry phase, Nat. Phys. **12**, 191 (2016).
[15] B. E. Feldman, M. T. Randeria, A. Gyenis, F. Wu, H. Ji, R. J. Cava, A. H. MacDonald, and A. Yazdani, Observation of a nematic quantum Hall liquid on the surface of bismuth, Science **354**, 316 (2016).
[16] A. Stern, Anyons and the quantum Hall effect—A pedagogical review, Ann. Phys. (N.Y.) **323**, 204 (2008).
[17] H. Bartolomei *et al.*, Fractional statistics in anyon collisions, Science **368**, 173 (2020).
[18] M. Banerjee, M. Heiblum, V. Umansky, D. E. Feldman, Y. Oreg, and A. Stern, Observation of half-integer thermal Hall conductance, Nature (London) **559**, 205 (2018).
[19] Y. P. Shkolnikov, S. Misra, N. C. Bishop, E. P. De Poortere, and M. Shayegan, Observation of quantum Hall "valley skyrmions", Phys. Rev. Lett. **95**, 066809 (2005).
[20] S. S. Hegde and I. S. Villadiego, Theory of competing charge density wave, Kekulé, and antiferromagnetically ordered fractional quantum Hall states in graphene aligned with boron nitride, Phys. Rev. B **105**, 195417 (2022).
[21] Y. Barlas, R. Côté, and M. Rondeau, Quantum Hall to charge-density-wave phase transitions in (*ABC*)-trilayer graphene, Phys. Rev. Lett. **109**, 126804 (2012).
[22] S. A. Vitale, D. Nezich, J. O. Varghese, P. Kim, N. Gedik, P. Jarillo-Herrero, D. Xiao, and M. Rothschild, Valleytronics: Opportunities, challenges, and paths forward, Small **14**, 1801483 (2018).
[23] J. R. Schaibley, H. Yu, G. Clark, P. Rivera, J. S. Ross, K. L. Seyler, W. Yao, and X. Xu, Valleytronics in 2D materials, Nat. Rev. Mater. **1**, 16055 (2016).
[24] A. Rycerz, J. Tworzydło, and C. W. J. Beenakker, Valley filter and valley valve in graphene, Nat. Phys. **3**, 172 (2007).
[25] S. Goswami *et al.*, Controllable valley splitting in silicon quantum devices, Nat. Phys. **3**, 41 (2007).
[26] O. Gunawan, Y. P. Shkolnikov, K. Vakili, T. Gokmen, E. P. De Poortere, and M. Shayegan, Valley susceptibility of an interacting two-dimensional electron system, Phys. Rev. Lett. **97**, 186404 (2006).
[27] M. Shayegan, K. Karrai, Y. P. Shkolnikov, K. Vakili, E. P. De Poortere, and S. Manus, Low-temperature, *in situ* tunable, uniaxial stress measurements in semiconductors using a piezoelectric actuator, Appl. Phys. Lett. **83**, 5235 (2003).
[28] J. Isberg, M. Gabrysch, J. Hammersberg, S. Majdi, K. K. Kovi, and D. J. Twitchen, Generation, transport and detection of valley-polarized electrons in diamond, Nat. Mater. **12**, 760 (2013).
[29] T. Ando, A. B. Fowler, and F. Stern, Electronic properties of two-dimensional systems, Rev. Mod. Phys. **54**, 437 (1982).
[30] K. Eng, R. N. McFarland, and B. E. Kane, Integer quantum Hall effect on a six-valley hydrogen-passivated silicon (111) surface, Phys. Rev. Lett. **99**, 016801 (2007).
[31] M. P. Losert, M. A. Eriksson, R. Joynt, R. Rahman, G. Scappucci, S. N. Coppersmith, and M. Friesen, Practical strategies for enhancing the valley splitting in Si/SiGe quantum wells, Phys. Rev. B **108**, 125405 (2023).
[32] Y. Shimazaki, M. Yamamoto, I. V Borzenets, K. Watanabe, T. Taniguchi, and S. Tarucha, Generation and detection of pure valley current by electrically induced Berry curvature in bilayer graphene, Nat. Phys. **11**, 1032 (2015).
[33] M. S. Mrudul, Á. Jiménez-Galán, M. Ivanov, and G. Dixit, Light-induced valleytronics in pristine graphene, Optica **8**, 422 (2021).
[34] J.-X. Li, W.-Q. Li, S.-H. Hung, P.-L. Chen, Y.-C. Yang, T.-Y. Chang, P.-W. Chiu, H.-T. Jeng, and C.-H. Liu, Electric control of valley polarization in monolayer WSe_2 using a van der Waals magnet, Nat. Nanotechnol. **17**, 721 (2022).
[35] E. J. Sie, J. W. McIver, Y.-H. Lee, L. Fu, J. Kong, and N. Gedik, Valley-selective optical stark effect in monolayer WS_2, Nat. Mater. **14**, 290 (2015).
[36] Y. Liu, Y. Gao, S. Zhang, J. He, J. Yu, and Z. Liu, Valleytronics in transition metal dichalcogenides materials, Nano Res. **12**, 2695 (2019).
[37] L. Zhao, J. Wang, B.-L. Gu, and W. Duan, Tuning surface Dirac valleys by strain in topological crystalline insulators, Phys. Rev. B **91**, 195320 (2015).
[38] G. Krizman, B. A. Assaf, M. Orlita, G. Bauer, G. Springholz, R. Ferreira, L. A. de Vaulchier, and Y. Guldner, Interaction between interface and massive states in multivalley topological heterostructures, Phys. Rev. Res. **4**, 013179 (2022).
[39] G. Krizman, B. A. Assaf, T. Phuphachong, G. Bauer, G. Springholz, G. Bastard, R. Ferreira, L. A. de Vaulchier, and Y. Guldner, Tunable Dirac interface states in topological superlattices, Phys. Rev. B **98**, 075303 (2018).
[40] M. M. Hasegawa, E. A. de Andrada e Silva, and G. C. La Rocca, Electron-hole symmetry and spin-orbit splitting in IV-VI asymmetric quantum wells, Physica (Amsterdam) **20E**, 400 (2004).
[41] F. S. Pena, S. Wiedmann, E. Abramof, D. A. W. Soares, P. H. O. Rappl, S. de Castro, and M. L. Peres, Quantum Hall effect and Shubnikov–de Haas oscillations in a high-mobility *p*-type PbTe quantum well, Phys. Rev. B **103**, 205305 (2021).
[42] V. A. Chitta, W. Desrat, D. K. Maude, B. A. Piot, N. F. Oliveira, P. H. O. Rappl, A. Y. Ueta, and E. Abramof, Multivalley transport and the integer quantum Hall effect in a PbTe quantum well, Phys. Rev. B **72**, 195326 (2005).
[43] M. M. Olver, J. Z. Pastalan, S. E. Romaine, B. B. Goldberg, G. Springholz, G. Ihninger, and G. Bauer, The observation of the integral quantum Hall effect in $PbTe/Pb_{1-x}Eu_xTe$ quantum well structures, Solid State Commun. **89**, 693 (1994).
[44] See Supplemental Material at http://link.aps.org/supplemental/10.1103/PhysRevLett.132.166601 for additional information on x-ray strain determination, k.p calculations, magneto-optics of all samples and further magnetotransport analysis.
[45] V. V Volobuev *et al.*, Giant Rashba splitting in $Pb_{1-x}Sn_xTe$ (111) topological crystalline insulator films controlled by Bi doping in the bulk, Adv. Mater. **29**, 1604185 (2017).
[46] Y. Zhang, Y.-W. Tan, H. L. Stormer, and P. Kim, Experimental observation of the quantum Hall effect and Berry's phase in graphene, Nature (London) **438**, 201 (2005).
[47] M. O. Goerbig, Electronic properties of graphene in a strong magnetic field, Rev. Mod. Phys. **83**, 1193 (2011).
[48] J Singleton, E Kress-Rogers, A V Lewis, R J Nicholas, E J Fantner, G Bauer, and A Otero, Magneto-optical studies of strained PbTe, J. Phys. C **19**, 77 (1986).

[49] I. I. Zasavitskii, E. A. de Andrada e Silva, E. Abramof, and P. J. McCann, Optical deformation potentials for PbSe and PbTe, Phys. Rev. B **70**, 115302 (2004).
[50] G. Lippmann, P. Kästner, and W. Wanninger, Elastic constants of PbSe, Phys. Status Solidi (a) **6**, K159 (1971).
[51] P. Enders, Acoustic and optical deformation potentials in cubic IV-VI compounds, Phys. Status Solidi (b) **132**, 165 (1985).
[52] S. Rabii, Investigation of energy-band structures and electronic properties of PbS and PbSe, Phys. Rev. **167**, 801 (1968).
[53] M. Simma, G. Bauer, and G. Springholz, Band alignments and strain effects in $PbTe/Pb_{1-x}Sr_xTe$ and $PbSe/Pb_{1-x}Sr_xSe$ quantum-well heterostructures, Phys. Rev. B **90**, 195310 (2014).
[54] G. Krizman, B. A. Assaf, T. Phuphachong, G. Bauer, G. Springholz, L. A. de Vaulchier, and Y. Guldner, Dirac parameters and topological phase diagram of $Pb_{1-x}Sn_xSe$ from magnetospectroscopy, Phys. Rev. B **98**, 245202 (2018).
[55] P. Dziawa *et al.*, Topological crystalline insulator states in $Pb_{1-x}Sn_xSe$, Nat. Mater. **11**, 1023 (2012).
[56] C.-Z. Li, J.-G. Li, L.-X. Wang, L. Zhang, J.-M. Zhang, D. Yu, and Z.-M. Liao, Two-carrier transport induced Hall anomaly and large tunable magnetoresistance in Dirac semimetal Cd_3As_2 nanoplates, ACS Nano **10**, 6020 (2016).
[57] E. E. Mendez, L. Esaki, and L. L. Chang, Quantum Hall effect in a two-dimensional electron-hole gas, Phys. Rev. Lett. **55**, 2216 (1985).
[58] K. Suzuki, K. Takashina, S. Miyashita, and Y. Hirayama, Landau-level hybridization and the quantum Hall effect in InAs/AlSb/GaSb electron-hole systems, Phys. Rev. Lett. **93**, 016803 (2004).
[59] R. J. Nicholas, K. Takashina, M. Lakrimi, B. Kardynal, S. Khym, N. J. Mason, D. M. Symons, D. K. Maude, and J. C. Portal, Metal-insulator oscillations in a two-dimensional electron-hole system, Phys. Rev. Lett. **85**, 2364 (2000).
[60] D. A. Abanin, K. S. Novoselov, U. Zeitler, P. A. Lee, A. K. Geim, and L. S. Levitov, Dissipative quantum Hall effect in graphene near the Dirac point, Phys. Rev. Lett. **98**, 196806 (2007).
[61] S. Das Sarma and K. Yang, The enigma of the $N = 0$ quantum Hall effect in graphene, Solid State Commun. **149**, 1502 (2009).
[62] A. Das, R. K. Kaul, and G. Murthy, Coexistence of canted antiferromagnetism and bond order in $\mathrm{Nu} = 0$ graphene, Phys. Rev. Lett. **128**, 106803 (2022).